ELSEVIER

Physica D 126 (1999) 145–159

PHYSICA D

A two parameter family of travelling waves with a singular barrier arising from the modelling of extracellular matrix mediated cellular invasion

Abbey J. Perumpanani [a,b], Jonathan A. Sherratt [c,*], John Norbury [d], Helen M. Byrne [e]

[a] *Mathematics Institute, University of Warwick, Coventry CV4 7AL, UK*
[b] *Department of Surgery, Harvard Medical School, Bldg 1400 W, One Kendall Square, Cambridge, MA 02139, USA*
[c] *Department of Mathematics, Heriot-Watt University, Edinburgh EH14 4AS, UK*
[d] *Mathematical Institute, University of Oxford, 24-29 St.Giles', Oxford OX3 9DU, UK*
[e] *Department of Theoretical Mechanics, University of Nottingham, University Park, Nottingham NG7 2RD, UK*

Received 25 May 1998; received in revised form 18 August 1998; accepted 1 October 1998
Communicated by F.H. Busse

Abstract

Invasive cells variously show changes in adhesion, protease production and motility. In this paper the authors develop and analyse a model for malignant invasion, brought about by a combination of proteolysis and haptotaxis. A common feature of these two mechanisms is that they can be produced by contact with the extracellular matrix through the mediation of a class of surface receptors called integrins. An unusual feature of the model is the absence of cell diffusion. By seeking travelling wave solutions the model is reduced to a system of ordinary differential equations which can be studied using phase plane analysis. The authors demonstrate the presence of a singular barrier in the phase plane and a "hole" in this singular barrier which admits a phase trajectory. The model admits a family of travelling waves which depend on two parameters, i.e. the tissue concentration of connective tissue and the rate of decay of the initial spatial profile of the invading cells. The slowest member of this family corresponds to the phase trajectory which goes through the "hole" in the singular barrier. Using a power series method the authors derive an expression relating the minimum wavespeed to the tissue concentration of the extracellular matrix which is arbitrary. The model is applicable in a wide variety of biological settings which combine haptotaxis with proteolysis. By considering various functional forms the authors show that the key mathematical features of the particular model studied in the early parts of the paper are exhibited by a wider class of models which characterise the behaviour of invading cells.

Keywords: Cancer; Invasion; Melanoma; Metastasis; Travelling waves

1. Introduction

Malignant tumours spread into neighbouring tissue following the acquisition of an invasive phenotype which can be separated into three main characteristics: adhesion, local proteolysis and migration. Adhesion is of two types:

* Corresponding author. Tel.: +44-0131-449-5111; e-mail: jas@ma.hw.ac.uk

0167-2789/99/$ – see front matter
PII: S0167-2789(98)00272-3

homotypic adhesion, in which a cell sticks to other cells of its own kind, results in a decreased tendency to invade surrounding tissue; and heterotypic adhesion, in which cells stick to connective tissue elements, and hence, move into surrounding tissue. Increased heterotopic adhesion may therefore favour invasion. Invading tumour cells also produce proteases which help digest surrounding connective tissue elements, thereby promoting invasion. Since normal cells are also capable of producing proteins which can inhibit the activity of these proteases, and hence, provide protection from invasion, there is a dynamic interplay between proteases and anti-proteases. The migration of cells is in general both random and directed. When random movement is augmented by chemical mediators it is called chemokinetic movement. Directed movement can occur in response to a diffusible substrate (chemotaxis) or in response to a fixed substrate (haptotaxis). An interplay of these phenotypic features in a rapidly proliferating cell causes malignant invasion, although not all the features are simultaneously necessary.

In this paper we consider the consequences of the concurrent induction of proteolysis and haptotaxis by a matrix component such as type IV collagen. Typically this induction is brought about through integrins, which are transmembrane adhesion molecules expressed on the cell surface that play an important role in the invasion. Seftor et al. [1] showed that the stimulation of the integrin receptor ($\alpha_V\beta_3$) in the human melanoma cell line A375M with either polyclonal or monoclonal anti-$\alpha_V\beta_3$ antibodies resulted in stimulation of invasion through basement membrane matrices in vitro. They also showed that cells treated with anti-$\alpha_V\beta_3$ antibody showed higher levels of both the secreted 72 kDa enzyme and its mRNA. They hence concluded that signal transduction through the $\alpha_V\beta_3$ integrin could underlie the elevated expression of metalloproteinase and the enhanced invasion of A375M cells through the basement membrane matrices. A similar signal transduction induced by matrix molecules in tumour cells was reported by Aznavoorian et al. [2] to induce chemotaxis and haptotaxis in A2058 human melanoma cells. They were able to induce cellular migratory responses using laminin, fibronectin and type IV collagen. Using checkerboard analysis they demonstrated that the migration of the cells was predominantly directional and that the random movement (chemokinetic component) was minimal. Another interesting observation they made was that pertusis toxin profoundly inhibited the chemotactic response to type IV collagen. This limited cellular migration to haptotactic movement.

Previous models of cell motility in the context of tumour biology have focussed on angiogenesis. For instance Chaplain and Stuart [3] have modelled the chemotactic movement of endothelial cells in tumour angiogenesis. In this paper we study the effects on malignant cells of haptotaxis, as shown in A2058 cells by Aznavoorian et al. [2], and protease production, as shown in A375 cells by Seftor et al. [1] (see Fig. 1) .

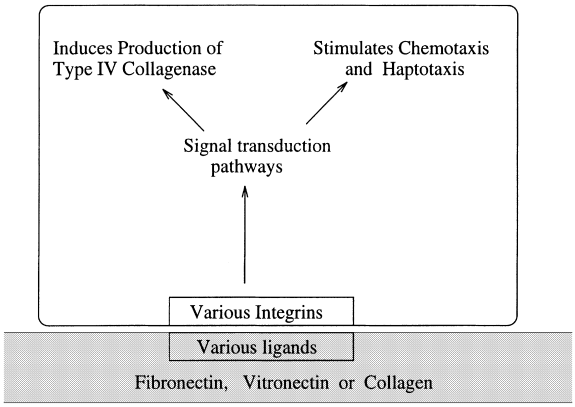

Fig. 1. Contact of the melanoma cell with ECM molecules results in the induction of multiple signal transduction pathways resulting in invasion. Seftor et al. [1] demonstrated an increased matrix degradation which is at least partly due to the increased expression of the matrix degrading enzyme, 72-kd type IV collagenase in the human melanoma cell line A375M. Aznavoorian et al. [2] also showed the stimulation of chemotaxis and haptotaxis resulting from contact with ECM molecules in A2058 human melanoma cell line.

2. The model

We derive a model for invasion by haptotaxis and proteolysis based on a continuum approach in which $u(x,t)$, $c(x,t)$ and $p(x,t)$ represent the concentrations of the invasive cells, extracellular matrix and protease. Here x and t are the space and time coordinates. The model studies the averaged behaviour of the melanoma cells in the direction of invasion only and ignores variations in the plane perpendicular to the direction of invasion.

Invasive cells. In studying malignant invasion we are concerned with the spatial movement of the cells and their proliferation. We model the spatial dynamics by considering directed cell movement up an extracellular matrix gradient $\partial c/\partial x$. This models the behaviour of A2058 cells after treatment with pertusis toxin as reported by Aznavoorian et al. [2] and leads to a haptotactic cell movement term of the form $\partial/\partial x(u\partial c/\partial x)$ where the flux of the tumour cells is proportional to $u\partial c/\partial x$. In their experiments Aznavoorian et al. [2] reported minimal chemokinetic movement and correspondingly a key feature of this model is the absence of a term for random cell motility.

The increased proliferation of malignant cells relative to normal cells is an important feature of tumour dynamics. We initially model this as a logistic type growth of the form $k_1u(k_2-u)$ which has been shown by Vaidya and Alexandro Jr. [7] to describe adequately the growth of human tumours grown by Schwartz [8]. In Section 6 we consider the effects of choosing other functional forms to describe tumour growth.

Extracellular matrix. Since extracellular matrix elements are much longer than cells, their motility is negligible compared to the movement of the malignant cells and the protease. We hence model the dynamics of connective tissue as a simple passive degradation by the activity of the tissue proteases; we describe this proteolysis by $-g(c,p)$, since it depends on the amount of collagen c still present as well as the protease p.

Proteases. The production of proteases is tightly confined to the interface between an invading tumour and the receding connective tissue. In some instances it is possible to localise the interstitial collagenase production to the stromal fibroblasts immediately adjacent to the site of tumour invasion, which suggests that invasive cells release a stimulus for induction of interstitial collagenase by fibroblasts. Nabeshima et al. [4] have characterised and sequenced a tumour cell derived collagenase stimulatory factor. However, there are other explanations for the production of the protease only at the invading front. Xie et al. [5] have shown the density dependent induction of 92-kd type IV collagenase activity in cultures of A431 human epidermoid carcinoma cells. They showed that only dividing cells stained positive when treated with anti-MMP antibodies and hence that only noncontact-inhibited tumour cells produce protease. Many proteases are predominantly membrane bound (e.g. uroplasminogen activator), but even when the protease is secreted into the extracellular space, activation has been shown to occur only on the cell surface, so that the behaviour closely resembles that for membrance bound proteases [6]. Thus we do not include protease diffusion in our model. We introduce the function $h(u,c)$ to represent the dependence of this tightly regulated protease production on the local concentrations of the melanoma cells and collagen. In addition we assume that the protease decays linearly, with half-life K.

Combining the above, we now write the model as

$$\frac{\partial u}{\partial t} = \overbrace{f(u)}^{\text{invasive cell proliferation}} - \overbrace{k_3\frac{\partial}{\partial x}\left[u\frac{\partial c}{\partial x}\right]}^{\text{haptotactic cell movement}}, \tag{1a}$$

$$\frac{\partial c}{\partial t} = -g(c,p) \;\}_{\text{proteolysis}}, \tag{1b}$$

$$\frac{\partial p}{\partial t} = \underbrace{h(u,c)}_{\text{protease prod}^n} - \underbrace{Kp}_{\text{natural decay}}, \tag{1c}$$

where f, g and h are increasing functions of u, c and p. Compared to previous work on the modelling of cell movement, this model is unusual in that there is no cellular diffusion. This case has been considered previously by

Rascle and Ziti [9] in the very different context of cellular aggregation, where they obtained conditions for blow-up in the absence of cell kinetics.

Before continuing with our model analysis, we eliminate p from the model equations as follows. The timescales associated with protease production and protease decay are much shorter than a typical timescale for the invading cells (see [10] for a review of timescales of protease activity). Hence writing $h(u, c) = K\bar{h}(u, c)$, where we assume $K \gg 1$, and multiplying through Eq. (1c) by the small parameter K^{-1}, we deduce that to leading order $p = \bar{h}(u, c)$. Henceforth no reference to p is needed: this expression may be used to eliminate p from Eqs. (1a) and (1b). This type of quasi-steady state assumption is a common one in enzyme kinetics [11], and numerical simulations of the three Eqs. (1a)–(1c) compare well with the simplified system of two equations; the great advantage of the two equation case is that it is amenable to detailed mathematical analysis.

Initially we examine the model using the simple functional forms

$$f(u) = k_1 u(k_2 - u), \qquad g(c, p) = k_4 pc, \qquad h(u, c) = k_5 uc. \tag{2}$$

In Section 6 we demonstrate that the qualitative behaviour of the model is not crucially dependent on any of the functional forms we have chosen. Any biologically reasonable functions characterising the behaviour of the cells, connective tissue and proteases we have already mentioned will demonstrate the features we describe.

2.1. Nondimensionalisation

After making the substitutions for f, g and h from (2) into Eqs. (1a)–(1c) and eliminating p using $p = h(u, c)$ we nondimensionalise the resulting equations using

$$\hat{u} = \frac{u}{u^*}, \quad \hat{c} = \frac{c}{c^*}, \quad \hat{t} = \frac{t}{T}, \quad \hat{x} = \frac{x}{L}, \quad L = \left[\frac{k_3}{k_2 k_4 k_5}\right]^{1/2}, \quad T = \frac{1}{k_1 k_2}, \quad u^* = k_2, \quad c^* = \frac{k_1}{k_4 k_5}.$$

Dropping $\hat{}$s for notational convenience then gives rise to the system

$$\frac{\partial u}{\partial t} = u(1 - u) - \frac{\partial}{\partial x}\left[u\frac{\partial c}{\partial x}\right], \tag{3a}$$

$$\frac{\partial c}{\partial t} = -uc^2. \tag{3b}$$

2.2. Spatially homogeneous system

Setting $\partial/\partial x = 0$ in (3a) we remark that the spatially homogeneous system has two steady states

(i) $u = 0$, c arbitrary: this is a continuum of (unstable) steady states parametrised by the (variable) amount of connective tissue in different tissues.

(ii) $u = 1$, $c = 0$: this (stable) steady state corresponds to complete replacement of the normal tissue by invading malignant cells.

With $\partial/\partial x = 0$, (3a) and (3b) can be solved explicitly giving

$$u(t) = [1 + \exp(-t + c_2)]^{-1}, \tag{4a}$$

$$c(t) = [t - c_1 + \log\{1 + \exp(-t + c_2)\}]^{-1}, \tag{4b}$$

where c_1 and c_2 are arbitrary constants. The behaviour as $t \to \infty$ shows that $u \to 1$ and $c \to 0$, hence justifying our classification of the steady state $(u, c) = (1, 0)$ as stable.

2.3. Classification of Eqs. (3a) and (3b)

Since the system (3a) and (3b) is of a nonstandard form we first discuss its type and the appropriate initial/boundary conditions. To show that the general system (3a) and (3b) is hyperbolic we differentiate (3b) with respect to t and substitute exactly for u_t and c_t in the right-hand side, which gives a nonlinear wave equation for c. To proceed more rigorously, we rewrite (3a) and (3b) as a system of first order equations by introducing $\gamma(x,t) \equiv c_x$, giving

$$\frac{\partial}{\partial t}\begin{bmatrix} u \\ \gamma \\ c \end{bmatrix} + \begin{bmatrix} \gamma & u & 0 \\ c^2 & 0 & 0 \\ 0 & 0 & 0 \end{bmatrix} \frac{\partial}{\partial x}\begin{bmatrix} u \\ \gamma \\ c \end{bmatrix} + \begin{bmatrix} u^2 - u \\ 2uc\gamma \\ uc^2 \end{bmatrix} = \begin{bmatrix} 0 \\ 0 \\ 0 \end{bmatrix}. \tag{5}$$

The 3×3 matrix in this equation has eigenvalues $\lambda_1 = 0$ and $\lambda_2, \ \lambda_3 = \frac{1}{2}[\gamma \pm (\gamma^2 + 4c^2u)^{1/2}]$, which are real and distinct (implying that the equations are hyperbolic) provided that $u \geq 0$. Now, provided that $u \geq 0$ initially, this will remain so, because if $u = 0$ at some point $x = x_0$ with $u \geq 0$ elsewhere, then u_x must also be zero at $x = x_0$, so that u remains zero and never becomes negative. Thus provided $u \geq 0$ initially, the system (3a) and (3b) is purely hyperbolic. It follows that the Cauchy problem can be solved provided the initial data (specifically the values of u, c and $\gamma \equiv c_x$) are specified on a curve that does not touch a characteristic. Since the characteristics are given by $\partial x/\partial t = \lambda_i (i = 1, 2, 3)$, they always have a finite gradient in the $x - t$ plane and thus specifying data on $t = 0$ is appropriate. In this discussion we consider the case in which the spatial domain is the whole real line. The Cauchy problem for reaction–convection equations in higher-dimensional spaces has been discussed by Lu [12].

3. Travelling wave analysis

Intuitively one expects the invasion process to correspond to travelling wave solutions of the model (3a) and (3b) with the normal tissue steady state $u = 0$ ahead of the wave and the fully malignant state $u = 1$, $c = 0$ behind the wave. This is confirmed by numerical solutions of (3a) and (3b), which will be discussed in more detail below (Section 4). Such travelling wave solutions can be studied analytically using the travelling wave differential equations. We look for constant shape travelling wavefront solutions of (3a) and (3b) by setting

$$u(x,t) = U(z), \qquad c(x,t) = C(z), \qquad z = x - at, \tag{6}$$

where a is the positive wavespeed which has to be determined. When solutions of the type (6) exist they represent travelling waves moving in the positive x-direction. Substitution of (6) into (3a) and (3b) followed by simple algebraic manipulation gives

$$\frac{\mathrm{d}U}{\mathrm{d}z}\left[-a + \frac{2UC^2}{a}\right] = U(1-U) - \frac{2U^3C^3}{a^2}, \tag{7a}$$

$$\frac{\mathrm{d}C}{\mathrm{d}z} = \frac{UC^2}{a}. \tag{7b}$$

The analysis of (7a) and (7b) involves the study of the (U, C) phase plane. Since we are looking for travelling waves connecting $(1, 0)$ and $(0, \hat{C})$ in the (U, C) phase plane we look for solutions of (7a) and (7b) with boundary conditions

$$U(-\infty) = 1, \quad C(-\infty) = 0, \quad U(\infty) = 0, \quad C(\infty) = \hat{C}, \tag{8}$$

which requires $(1, 0)$ to have an unstable manifold while $(0, \hat{C})$ must have a stable manifold. In order to study this we look at the stability of the system (7a) and (7b).

3.1. Stability analysis

The steady states (U_0, C_0) of (7a) and (7b) are $(0, \hat{C})$ and $(1, 0)$, where $\hat{C}$ represents a continuum of steady states. We study their stability by looking at the eigenvalues of the stability matrix linearised about the steady states. The eigenvalues about $(0, \hat{C})$ are $-1/a$ and 0. The corresponding eigenvectors are $(1, -\hat{C})$ and $(0, 1)$. The negative eigenvalue indicates that there is a stable manifold along $(1, -\hat{C})$. The zero eigenvalue represents translations along the continuum of steady states.

The eigenvalues about $(1, 0)$ are $1/a$ and 0. The eigenvector corresponding to $1/a$ is $(1, 0)$ and represents movement along the u axis. The eigenvector corresponding to the zero eigenvalue is $(0, 1)$ which is in the direction perpendicular to the u axis. Numerical solutions of (7a) and (7b) show that the trajectory leaving this steady state leave along the eigenvector corresponding to the zero eigenvalue of the linearised system. This zero eigenvalue comes from (7b). In order to get a clearer picture of the behaviour close to $(1, 0)$ we look at the nonlinear terms in (7b). One method to do this is to use the techniques of centre manifold theory which shows that as $z \to -\infty$, $U(z)$ approaches 1 exponentially while $C(z)$ tends zero as z^{-1}.

The existence of an unstable manifold about $(0, \hat{C})$ as $z \to \infty$ and a stable centre manifold about $(1, 0)$ as $z \to -\infty$ is consistent with the existence of a travelling wave orbit connecting the two steady states. We now proceed to investigate this connection.

3.2. Phase plane analysis

3.2.1. The singular barrier

Referring to (7a) and (7b) we remark that $\mathrm{d}C/\mathrm{d}U = 0$ on the curve

$$a^2 - 2UC^2 = 0. \tag{9}$$

Along this curve equation (7a) becomes singular and the usual criteria of existence and uniqueness of solutions do not hold. We call this wall of singularities a "barrier". The phase paths have meaning only on either side of this barrier. However, at the point that this singular barrier is crossed by the u nullcline

$$U(1 - U) - \frac{2U^3C^3}{a^2} = 0, \tag{10}$$

the derivative is finite, so that there is the possibility of a phase path going through this point. We refer to this point as the "hole in the wall". By solving Eqs. (9) and (10) simultaneously the coordinates of this point $(U_{\mathrm{hole}}, C_{\mathrm{hole}})$ are given by

$$U_{\mathrm{hole}} = \frac{8a^2}{(a^2 + [8a^2 + a^4]^{1/2})^2}, \tag{11}$$

$$C_{\mathrm{hole}} = \frac{a^2 + [8a^2 + a^4]^{1/2}}{4}. \tag{12}$$

In Fig. 2 we show an example of the phase plane for a particular wavespeed a. The dotted line shows the wall of singularities defined by Eq. (9) and the dashed line shows the U nullcline described in Eq. (10). Through the point of their intersection there is a phase path that goes across the wall of singularities. We call this the "critical path". This critical path intersects the line $U = 0$ at a particular value of the haptotactic substrate concentration, $C = C_{\mathrm{crit},0}$, say.

3.2.2. A two parameter family of waves

Along the curve described by Eq. (9) $C \to 0$ as $U \to \infty$. Furthermore $(U_{\mathrm{hole}}, C_{\mathrm{hole}})$ and $(0, C_{\mathrm{crit},0})$ are connected by the critical path. This implies that for a given value of the wavespeed a, $(U = 0, C > C_{\mathrm{crit},0})$ cannot be connected

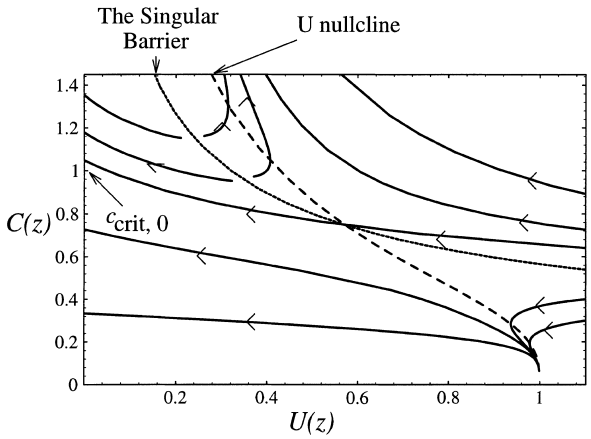

Fig. 2. Phase portrait for the system of equations (7a) and (7b). The dotted line, defined by Eq. (9), is the singular barrier to the phase trajectories. The interrupted line, defined by Eq. (10), is the U-nullcline of Eq. (7a). The point of intersection of the two lines is the "hole in the wall" whose coordinates are described by (11) and (12). In general, phase trajectories do not cross the singular barrier except at the "hole in the wall". We call this trajectory the "critical path". In this simulation we fix the wavespeed so that $a = 0.8$.

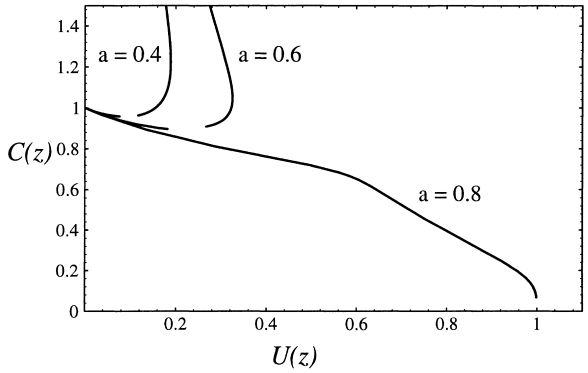

Fig. 3. Trajectories for different wavespeeds with a fixed initial conditions for the system of equations (7a) and (7b).The three curves correspond to phase paths with wavespeeds $a = 0.4$, 0.6 and 0.8. For wavespeeds below a critical minimum, there are no trajectories connecting the two steady states. The gap in the trajectories when $a = 0.4$ and $a = 0.6$ corresponds to the singular barrier; really we are showing the union of two trajectories, calculated on either side of the barrier.

to $(U = 1, C = 0)$ since phase paths neither cross each other nor the singular barrier. In other words, travelling wave solutions cannot exist for $\hat{C} > C_{\mathrm{crit},0}$. Furthermore for each given wavespeed there is the possibility of heteroclinic connections between $(U = 0, 0 < C < C_{\mathrm{crit},0})$ and $(U = 1, C = 0)$. We show such connections numerically in Fig. 2. For each positive wavespeed we demonstrate a family of travelling waves depending on the initial tissue concentration of the haptotactic substrate, which is bound above by $C_{\mathrm{crit},0}$.

On the other hand, given a particular initial concentration of the haptotactic substrate, trajectories with wavespeed below a critical $a_{\min}$ will not reach it and will instead connect a different part of the $U = 0$ line to $(U = 1, C = 0)$. However, we have observed numerically that for all wavespeeds above this minimum there are connections between the two steady states representing travelling wave solutions of (3a) and (3b). This demonstrates the presence of a family of travelling waves with respect to the wavespeed with a lower bound $a_{\min}$ for each point on $\hat{C}$. In Fig. 3 we present a phase plot for different values of a and show that for wavespeeds below a critical minimum there are no heteroclinic orbits given a level of substrate concentration.

Using (7a) and (7b) we can deduce the equation for $\mathrm{d}C/\mathrm{d}U$. Using $C(U_{\mathrm{hole}}) = C_{\mathrm{hole}}$ as an initial condition we can find $C_{\mathrm{crit},0}$ by integrating the equation for $\mathrm{d}C/\mathrm{d}U$ up to $U = 0$. This gives a relation between the minimum

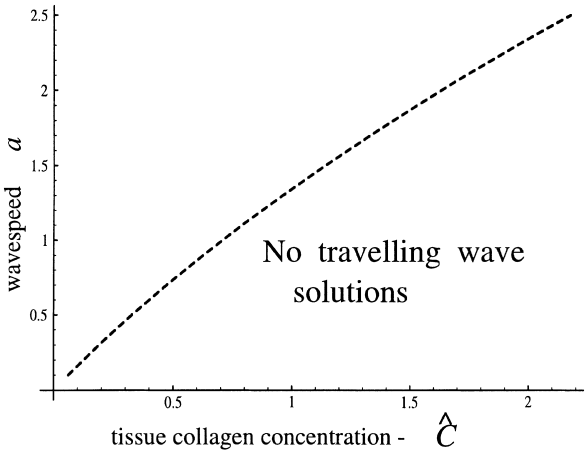

Fig. 4. An illustration of the domain in the $a - \hat{C}$ plane in which travelling wave solutions exist. Numerical solutions of (3a) and (3b) suggest that, for each value of $\hat{C}$, there is a family of waves whose wavespeed depends on the initial conditions. Of these, the wave with the minimum wavespeed appears to correspond to the trajectory, shown in Fig. 2, which passes through the "hole in the wall". The coordinates of this "hole in the wall" are given by (11) and (12). By integrating (15) from $U = U_{\text{hole}}$ to $U = 0$ we obtain the particular value of $\hat{C}$ corresponding to a given $a_{\min}$. For all values of a above $a_{\min}$, travelling wave solutions are possible, but for sets of $(a, \hat{C})$ below it there are no travelling wave solutions. The curve separating the two areas was computed numerically, using the method described above.

wavespeed $a_{\min}$ and $C_{\text{crit},0}$. This curve would divide the $(a, \hat{C})$ plane into two regions, one where travelling wave solutions are possible and another where travelling wave solutions do not exist. We demonstrate an example of this in Fig. 4.

4. Numerical solutions

We solved the original system of partial differential equations (3a) and (3b) using a flux limited Lax–Wendroff numerical scheme. Whereas our analysis refers to an infinite spatial domain, numerical solutions of course require a finite domain; we use Neumann boundary conditions at the ends of this domain, although Dirichlet conditions can also be used, with no significant effect on the solution provided the domain is sufficiently large. The solution evolved to travelling waves whose velocity depended on the choice of initial conditions (see Fig. 5). Decaying initial conditions ($u(x, 0) \propto \exp(-\xi x)$ for large x) gave rise to travelling waves whose velocity decreased as the rate of decay ξ of the initial conditions increased. However, for ξ above a critical value the wavespeed remains constant. The computed value of this minimum wavespeed was in good agreement with the minimum wavespeed predicted from the travelling wave analysis. Variations in initial conditions are of mathematical interest, but are of course of no biological relevance, and it is the minimum speed wave, corresponding to localised initial data, that is relevant biologically. In Fig. 6 we present an example of a minimum speed wave together with a faster wave obtained from the numerical solution. This form of wavespeed dependence of initial conditions is familiar from parabolic partial differential equations [11,13].

4.1. Stability of the travelling waves

In Fig. 4 we showed that for any given tissue concentration of the haptotactic substrate, $\hat{C}$, travelling wave solutions can exist for wavespeeds above a critical minimum. Further in Fig. 6, by choosing suitable initial conditions, we showed waves with speeds greater than the minimum predicted for that particular tissue concentration of the haptotactic substrate. An important issue now is the stability of these waves to small perturbations. A travelling

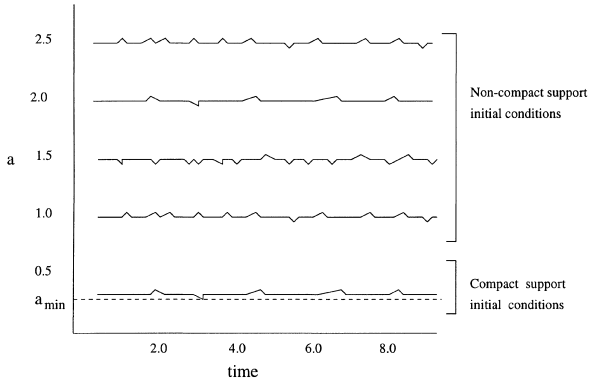

Fig. 5. A plot of the numerically calculated wavespeed against time for different initial conditions. In all cases the tissue concentration of the haptotactic substrate is fixed at $\hat{C} = 0.3$. In cases where decaying initial conditions are used wavespeeds increase as the rate of decay of the initial data decreases. However, for rapidly decaying initial data the wave evolves to one at the predicted minimum speed. The interrupted line shows the analytically predicted minimum wavespeed from the power series solutions. The continuous line overlying it is the solution for an initial condition with compact support.

wave solution is said to be stable if small spatially localised perturbations die out eventually or result in a mere phase shift of the solution.

There are two classes of perturbations that are relevant here – infinite domain perturbations and finite domain perturbations. We have shown numerically that the speed of propagation of the wavefront solutions depends on the behaviour of the initial conditions $u(x, 0)$ as $x \to \infty$ (see Fig. 6). This implies that the wavefront solutions are unstable to perturbations in the far field. On the other hand, if $u(x, 0)$ has compact support, that is

$$u(x, 0) = u_0(x) \geq 0, \qquad u_0(x) = 1 \quad \text{if } x \leq x_1, \qquad u_0(x) = 0 \quad \text{if } x \geq x_2, \tag{13}$$

then for some $x_2 > x_1$ the ultimate form of the numerically computed solution does not depend on the detailed form of $u(x, 0)$.

We now look at the role of finite domain perturbations. Analytical investigation of this is a substantial problem which we have not attempted. Instead we consider the problem of stability numerically. We solve the system (3a) and (3b) numerically using two different initial conditions $u_s(x, 0)$ and $u_p(x, 0) = u_s(x, 0) + w(x)$, where $w(x) \ll u_s(x, 0)$ and $w(x) = 0$ for $|x| > L$. We define $Pt(t)$ as

$$Pt(t) = \sum \left| u_s(x_i, t) - u_p(x_i, t) \right|, \tag{14}$$

where the sum is over all the points in the spatial mesh. For the wide variety of $w(x)$ we studied, $Pt(t)$ always decayed to zero. In Fig. 7 we present the evolution of $Pt(t)$ for two samples of $w(x)$. This figure also demonstrates that the faster waves shown in Fig. 6 are stable to a wide variety of perturbations.

5. Power series solutions

Eqs. (7a) and (7b) may be written in the form

$$\frac{\mathrm{d}C}{\mathrm{d}U} = \frac{UC^2(-a^2 + 2UC^2)}{a^2U(1-U) - 2U^3C^3}. \tag{15}$$

Equations such as (15) can be solved using the power series method. This involves expanding $C(U)$ in powers of U such that

$$C(U) = c_0 + c_1U + c_2U^2 + \cdots \tag{16}$$

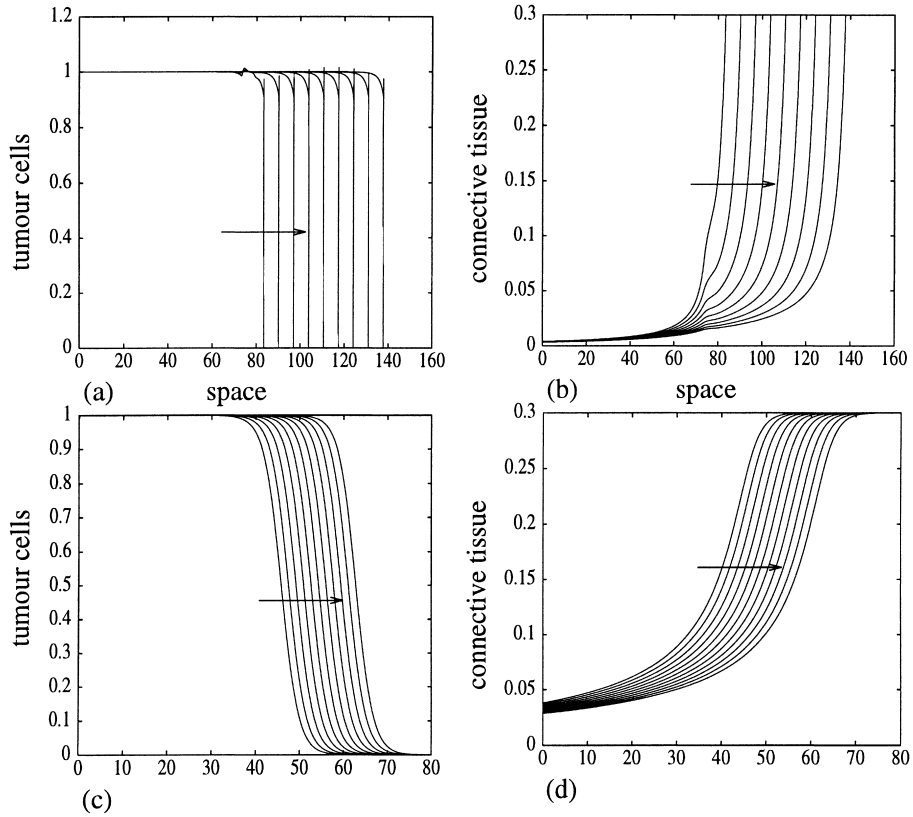

Fig. 6. Sketches showing the solutions of (3a) and (3b) for two choices of initial conditions, the solutions obtained using a finite difference scheme. In (a) and (b) we show the solutions for rapidly decaying initial conditions. Corresponding to the tumour cell wave there is a receding wave of connective tissue. The tissue concentration of the haptotactic substrate here is set to be 0.3. The computed wave velocity is 0.34. Using the method of integration from the "hole in the wall" described in the legend of Fig. 4, we estimate that the minimum wavespeed is 0.32. In (c) and (d) we show that, for the same tissue concentration of the haptotactic substrate, faster waves can be generated from slowly decaying initial conditions. The computed wave velocity in (c) and (d) is 1.9 which is considerably greater than the minimum wavespeed of 0.32. (Using different choices of slowly decaying initial conditions we have been able to generate an array of faster waves as shown in Fig. 5.) In (a) and (d) we plot u and c as functions of space x at equal intervals of time. The tumour cell wave has a steep front and there is a numerical artefact that decreases with the refinement of the mesh. However, even with very fine grids these artefacts cannot be eliminated completely.

By substituting (16) into (15) the coefficients of the power series $\{c_i\}_{i=1}^{\infty}$ can be sequentially defined in terms of c_0 to give

$$\begin{aligned} c_1 &= -c_0^2, \\ c_2 &= \frac{-a^2c_0^2 + 2a^2c_0^3 + 2c_0^4}{2a^2}, \\ c_3 &= \frac{c_0^2(-a^2 + 3a^2c_0 + 2c_0^2 - 3a^2c_0 - 12c_0^3)}{3a^2}, \\ &\vdots \end{aligned} \tag{17}$$

A key issue in such power series solutions is the convergence of the power series to the actual solution of the differential equation. For an equation of the form $\mathrm{d}u/\mathrm{d}c = F(u, c)$, the solution can be represented in the form of a convergent series about any point at which F is analytic.

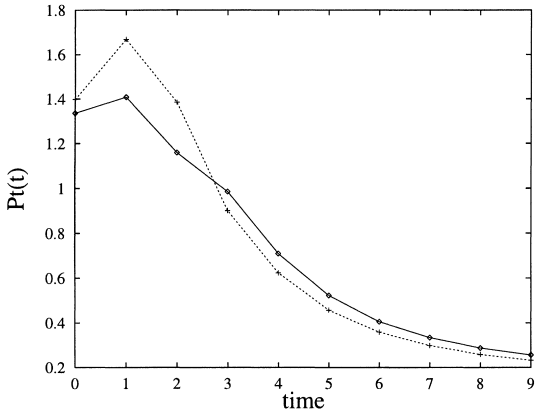

Fig. 7. A plot to show the decay of two finite domain perturbations to the numerical solution of (3a) and (3b). In the above figure we plot the evolution of a norm of the perturbations as defined by (14). For a wide variety of perturbations this norm decays to zero, indicating that these waves are stable. The decay appears to be exponential in all cases.

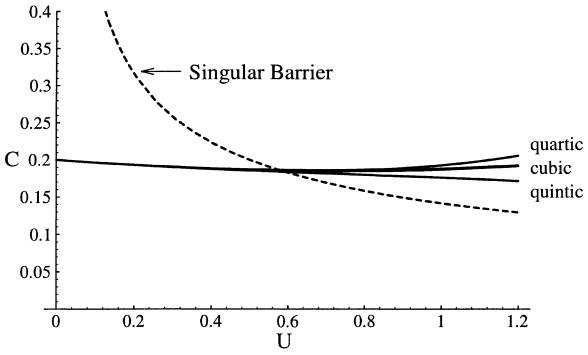

Fig. 8. A plot of the cubic, quartic and quintic partial sums of the polynomial described in (17) which is a power series solution of the ODE in (15). The interrupted curve is the wall of singularities defined in (9). Along this curve (15) is not analytic, and hence, the radius of convergence of the power series is bounded by this singular barrier.

In the (u, c) phase plane we described a curve given by (9) where the function F is not analytic. However, away from this curve F is analytic. In other words, we can obtain convergent power series approximations extending as far as the wall of singularities described in (9). In Fig. 8 we illustrate such a power series solution which is convergent up to the wall of singularities and divergent after crossing it. The different curves show solution approximations for the partial sums of (16) with quadratic, cubic, quartic and quintic terms.

A crucial issue in the solution of (7a) and (7b) is to determine the minimum wavespeed $a_{\min}$, as a function of c_0 the initial concentration of the haptotactic substrate. In (11) and (12) we described the coordinates of the hole in the wall, that is, the point through which the minimum wavespeed trajectory passes. Thus for a given initial concentration c_0 of the haptotactic substrate the power series solution through this point will satisfy

$$\frac{a_{\min}^2 + (8a_{\min}^2 + a_{\min}^4)^{1/2}}{4} = c_0 + \sum_{m=1}^{\infty} c_m U_{\text{hole}}^m, \tag{18}$$

where U_{hole} is given by (11) and the coefficients c_m are given in (17). The left-hand side is obtained from the c-coordinate of the hole in the wall described in (12). So by taking an adequate number of terms of the power series on the right-hand side of (18) we can obtain an implicit relation for $a_{\min}(c_0)$ to any required degree of accuracy.

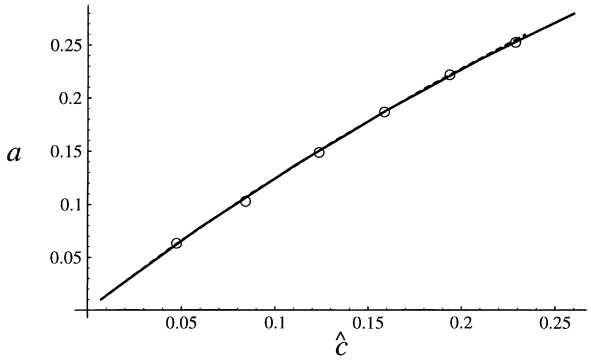

Fig. 9. Two sketches of the curve which partitions the $a - \hat{C}$ plane into regions in which travelling wave solutions do and do not exist. The continuous curve was constructed by numerical integration of (15) whereas the curve of open circles was constructed using the power series solution method. Thus along the continuous curve $C_{\text{crit},0}$ is obtained by integrating (15) with the initial condition $C(U_{\text{hole}}) = C_{\text{hole}}$ for various values of the wavespeed a. C_{hole} and U_{hole} are defined by Eqs. (11) and (12) and represent initial conditions corresponding to the "hole in the wall". The open circles show C_{hole} computed from the power series approximation described in (16) for various values of the wavespeed a. The power series was truncated at quadratic terms.

Table 1

Name of f	$f(u)$	$g(u, c)$
Gompertz	$k_1 u - k_2 u \log(u)$	$k_3 c$
von Bertalnaffy	$k_1 u^{2/3} - k_2 u$	$k_3 \exp(c)$
Generic	$k_1 u^{1-k_2 k_3} (k_4^{k_2} - u^{k_2})^{1+k_3} / k_4^{k_2}$	$k_5 c$
Piantadosi	$(k_1 u / (1 + k_2 u^{k_3})^{1/k_3}) - k_4 u$	$k_5 c(1 + u)$

In Fig. 9 we show such a curve obtained from (18) and compare it with the curve computed by integrating (15) numerically with the initial condition $U(C_{\text{hole}}) = U_{\text{hole}}$. The power series method thus yields a useful approximation for the minimum wavespeed as a function of the initial haptotactic substrate concentration.

6. Other functional forms

In order to demonstrate that both the biological and mathematical features of the model we describe are not a specific consequence of either the logistic growth model for the tumour cells or the specific choice of the degradative term for the connective tissue, we have considered several other functional forms for $f(u)$ and $g(u, c)$ in models of the form

$$\frac{\partial u}{\partial t} = f(u) - \frac{\partial}{\partial x}\left[u \frac{\partial c}{\partial x}\right], \tag{19}$$

$$\frac{\partial c}{\partial t} = -u g(u, c), \tag{20}$$

where $u(x, t)$ is, now, any invading species (e.g. placenta, a bacterial organism, etc.) and $c(x, t)$ any haptotractant that can be degraded (e.g. collagen, fibronectin, a nutrient source, etc.). For $f(u)$ we used functional forms that have been used to model tumour growth (Table 1).

In all cases these choices for f and g give the essential qualitative biological features described in Section 1, and numerical and analytical studies showed that they have the following features in common.

- Both the kinetic ODEs and the full PDEs possess a continuum of steady states for c about $u = 0$.

- In travelling wave coordinates, the $U - C$ phase plane possesses a curve

$$a^2 = 2Ug(U, C) + U^2 \frac{\mathrm{d}g}{\mathrm{d}U}, \tag{21}$$

  along which the U equation becomes singular and the usual criteria for existence and uniqueness of solutions do not hold for each positive wavespeed a.
- At the point where the U nullcline

$$f(U) = \frac{U^3 g(U, C)}{a^2} \frac{\mathrm{d}g}{\mathrm{d}C} \tag{22}$$

  intersects the curve in (21) the derivative $\mathrm{d}U/\mathrm{d}z$ is finite and hence admits a phase path going through this point. We call this phase path the "critical path".
- For a fixed wavespeed a the critical path intersects the line $U = 0$ at a point which we call $C_{\mathrm{crit},0}$. For all $0 < C < C_{\mathrm{crit},0}$ there are phase trajectories connecting a nonzero steady state of U with its trivial steady state and correspondingly the zero steady state of C with its continuum of nonzero steady states.
- For a fixed C there are travelling waves corresponding to all speeds above a critical minimum speed.
- The phase path of the travelling wave corresponding to the minimum speed wave goes through the point of intersection of (21) and (22) which we call the "hole in the wall".
- Numerical solutions suggest that the minimum speed wave corresponds to rapidly decaying initial conditions and that more slowly decaying initial conditions give rise to faster waves.

7. Discussion

We have described the travelling wave behaviour in a mathematical model of a cell type invading by a combination of haptotaxis and matrix degradation. Although we have focussed on the application of our model to metastatic tumour invasion, there are a number of other biological systems in which these two processes are the main regulators. For instance, in many mammals trophoblast cells of the placenta have acquired mechanisms to invade the uterus inclusive of its blood vessels, to establish efficient fetomaternal exchange of molecules. This invasion is strictly controlled both spatially and temporally, and in humans it usually continues until mid-gestation. Key mechanisms underlying various steps of trophoblast invasion are: (i) the attachment to the basement membrane, most probably by binding to laminin; (ii) the detachment from the basement membrane matrix, a process requiring the presence of complex-type oligosaccharides on the cell surface; and (iii) the breakdown of basement membrane components mediated by secretion of metalloproteases. A detailed review of these mechanisms is given by Graham and Lala [14]. Though the mechanisms are further regulated by TGF-β, in particular to bring about a cessation of invasion after adequate anchorage is achieved, the basic blueprint of the mechanism is that described in our model. A similar behaviour is also seen in bacteria growing in culture, where the bacteria move up gradients of nutrients.

Mathematically an unusual feature of this system is the absence of a term representing random cell motility. Numerical simulations suggest that if a small component of cell diffusion is added to the model, there is no significant change in either the form or speed of the travelling wave solutions corresponding to invasion, except that the derivative discontinuity in the u wave will of course be lost. However, mathematically such an extension profoundly alters the system, and investigation of this using perturbation theory is a natural candidate for future work. From a biological viewpoint, the absence of cellular diffusion is justified by experimental data indicating the overwhelming dominance of directed movement in cancer invasion [2]. Another natural extension of the work is to explicitly include protease kinetics, as in system (1a)–(1c). In this case, a number of the ideas generalise, in particular the existence of a singular barrier, which becomes a surface in the three-dimensional travelling wave space, with a line on this surface being analogous to the "hole in the wall". However, detailed analysis of the three-dimensional phase space is significantly more complicated than the two-dimensional case we have considered, and is again a

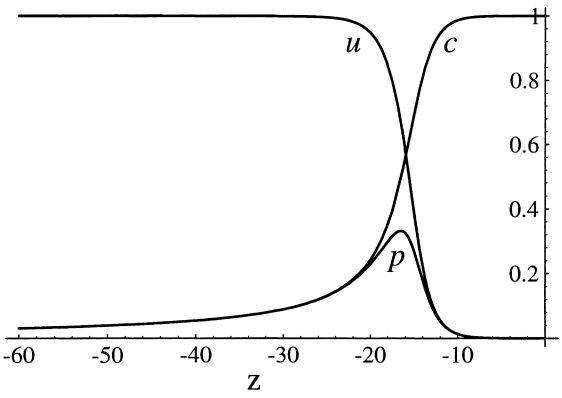

Fig. 10. Numerical solution of Eqs. (3a) and (3b). In travelling wave coordinates, the monotonically decreasing curve is the tumour cell wave in and the monotonically increasing curve is the connective tissue. For completeness, the corresponding protease profile is included ($p = h(u, c) = k_5uc$). As expected there is a pulse of protease confined chiefly to the interface of the tumour cell wave and the connective tissue.

natural area for future investigation. The presence of protease diffusion would further complicate the mathematics, although this would have little biological relevance, as discussed previously.

Using the nondimensionalisation described earlier the dimensional wavespeed is

$$a = a^* k_1 \left[\frac{k_2 k_3}{k_4 k_5}\right]^{1/2}, \tag{23}$$

where a^* is the nondimensional wavespeed. Here k_1 is the linear growth rate of the tumour cells, k_2 the carrying capacity, k_3 the coefficient of haptotaxis, k_4 the rate of proteolysis and k_5 is the rate of protease production. This precise prediction of invasion speed is the key biological outcome of this work. For example, it emerges from this formula that the more rapidly proliferating tumours would disseminate faster and that malignant cells with greater surface expression of heterotopic receptors (e.g. integrins) invade more aggressively. This confirms that the model is well behaved with respect to the known aspects of malignant invasion. Furthermore, although the model in (3a) and (3b) does not explicitly describe the behaviour of the protease, the distribution of the protease can be recovered using $p = h(u, c)$ and as expected it is chiefly confined to the interface of the advancing wave of tumour cells and the receding wave of connective tissue (Fig. 10).

In any application of this model to a real life situation, the issue of paramount interest would be the speed of invasion. In this model we have shown that the speed depends crucially on the tissue concentration of the haptotactic substrate, which would be fixed by the experimental protocol in an in vitro setting or the nature of the tissue in an in vivo setting. The power series approximation in (15) is therefore of practical interest, as it provides a measure of the invasiveness of a cell population as a function of the local extracellular matrix concentration. This measure may be used to determine the likelihood of metastasis for a given cancer and therefore the choice of therapeutic modality (e.g. between radiotherapy and surgical excision). Subsequent to the mathematical analysis we have presented, we performed a series of in vitro experiments for a particular cell–matrix system, namely the fibrosarcoma cell line HT1080 invading collagen gels. These experiments showed that the collagen density did indeed affect the speed of invasion: e.g. after 96 h the front of HT1080 cells invaded 4.19 mm into the gel at a collagen concentration of 0.936 mg/ml and 8.78 mm at 1.872 mg/ml. In the experimental system, invasiveness falls at extremely high collagen concentrations, due to physical effects of the collagen gel, which we do not consider in this paper. The direct relationship between invasion speed and moderate collagen densities is in agreement with the model prediction described by the power series in (16) and illustrated in Fig. 9. Moreover, the generality of the behaviour across a wide range of model formulations suggests that similar effects may be operative during other instances of directed cell migration such as placentation and angiogenesis.

Acknowledgements

AJP was supported by a Wellcome Trust Training Fellowship in mathematical biology and by a Harvard University Whittaker Fellowship. JAS and HMB were supported in part by grant GR/L41967 from the EPSRC (applied numerical mathematics programme). The work was partly funded by a grant from the London Mathematical Society (scheme 3). We thank Ben Marchant for helpful discussions.

References

[1] R.E. Seftor, E.A. Seftor, K.R. Gehlsen, W.G. Stetler-Stevenson, et al. Role of alpha-v-beta-3 integrin in human melanoma cell invasion, Proc. Natl. Acad. Sci. U.S.A. 89 (1992) 1557–1561.
[2] S. Aznavoorian, M.L. Stracke, H. Krutzsch, E. Schiffman, L.A. Liotta, Signal transduction for chemotaxis and haptotaxis by matrix molecules in tumour cells, J. Cell Biol. 110 (1990) 1427–1438.
[3] M.A.J. Chaplain, A.M. Stuart, A model mechanism for the chemotactic response of endothelial cells to tumour angiogenesis factor, IMA J. Math. Appl. Med. Biol. 10 (1993) 149–168.
[4] K. Nabeshima, W.S. Lane, C. Biswas, Partial sequencing and characterisation of the tumor cell-derived collagenase stimulatory factor, Arch. Biochem. Biophys. 285 (1991) 90–96.
[5] B. Xie, C.D. Bucana, I.J. Fidler, Density-dependent induction of 92-kd type type-IV collagenase activity in cultures of A431 human epidermoid carcinoma cells, Am. J. Pathol. 144 (1994) 1958–1967.
[6] Z. Werb, ECM and cell surface proteolysis: regulating cellular ecology, Cell 91 (1997) 439–442.
[7] V.G. Vaidya, F.J. Alexandro Jr., Evaluation of some mathematical models for tumour growth, Int. J. Biomed. Comput. 13 (1982) 19–35.
[8] M. Schwartz, A biomathematical approach to clinical tumour growth, Cancer 14 (1961) 1272.
[9] M. Rascle, C. Ziti, Finite time blow-up in some models of chemotaxis, J. Math. Biol. 33 (1995) 388–414.
[10] P. Mignatti, D.B. Rifkin, Biology and biochemistry of proteinases in tumor invasion, Physiol. Rev. 73 (1993) 161–195.
[11] J.D. Murray, Mathematical Biology, Springer, Berlin, 1990.
[12] V. Lu, The Cauchy problem for reaction–convection equations in higher dimensional spaces, Acta Math. Sci. 14 (1994) 332–336.
[13] J.A. Sherratt, On the transition from initial data to travelling waves in the Fisher-KPP equation, Dyn. Stab. Syst. 13 (1998) 167–174.
[14] C.H. Graham, P.K. Lala, Mechanisms of placental invasion of the uterus and their control, Biochem. Cell Biol. 70 (1992) 867–874.